Lawrence Berkeley Laboratory
UNIVERSITY OF CALIFORNIA

Materials & Molecular
Research Division

Submitted to Philosophical Transactions

THE FORMATION OF SUBSCALES OF VARYING COMPOSITIONS

D. P. Whittle, F. Gesmundo, B. D. Bastow and G. C. Wood

January 1980

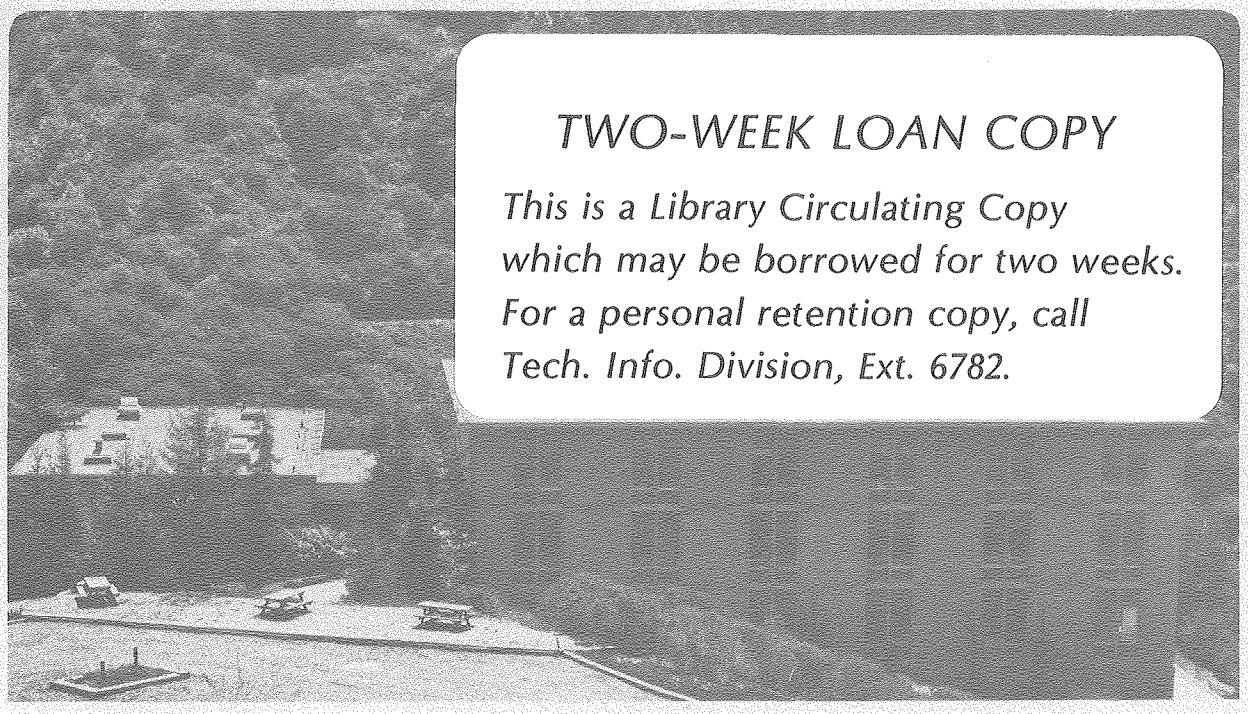

Prepared for the U.S. Department of Energy under Contract W-7405-ENG-48

DISCLAIMER

THE FORMATION OF SUBSCALES OF VARYING COMPOSITIONS

by

D. P. Whittle,[x] F. Gesmundo,[†] B. D. Bastow[*] and G. C. Wood[o]

[x]Lawrence Berkeley Laboratory, University of California
Berkeley, CA 94720, U.S.A.

[†]Centro Studi di Chimica Applicata, Consiglio Nazionale Della Richerche,
Genova, Italy

[*]British Nuclear Fuels Ltd., Windscale Works
Seascale, Cumbria, England

[o]Corrosion and Protection Centre, U.M.I.S.T.,
Manchester M60 1QD), England

To be submitted to Philosophical Transactions

October, 1979

CONTENTS

ABSTRACT

An earlier paper (Bastow et al., 1977) presented an analysis of the diffusion processes taking place in the surface scale when a binary alloy was oxidized and the resulting scale consisted of a solid solution of the oxides of the individual alloy components. However, it is shown here that if the diffusion of the oxidant into the alloy is significant then in addition to the formation of a surface scale, a subscale consisting of precipitate particles of the solid solution scale can form within the alloy. Unlike the classical cases of internal oxidation, the precipitated oxide is the same phase as the surface scale, although its composition is different and varies with depth below the surface. In addition, the fraction of precipitated subscale also varies with depth below the surface. Diffusion equations are established to describe these systems. The importance of the thermodynamic parameters, namely the relative stabilities of the two scale components, and the kinetic parameters, oxidant diffusivity in the alloy and overall growth rate of the scale, are demonstrated. The variation of subscale/surface scale thickness ratio with bulk alloy composition goes through a maximum at a value of the latter of around 0.1 - 0.2: this is largely related to the thermodynamics of the system.

ACKNOWLEDGEMENTS

A portion of this work has been supported by the Division of Materials Science, Office of Basic Energy Sciences, U.S. Department of Energy under Contract No. W-7405-Eng. 48.

LIST OF PRINCIPAL SYMBOLS

A, B	Metallic components in the alloy: B is assumed to be the component with the greater affinity for the oxidant.
AX, BX	Scale components.
a_X	Activity of the non-metallic oxidant, X.
a_X', a_X''	Activity of the oxidant, X, at the surface scale/alloy and surface scale/gas interfaces respectively.
D_{all}	Interdiffusion coefficient of the metallic components in the alloy.
D_B^o	Self-diffusion coefficient of B cations in pure BX at unit activity of X_2.
D_X	Diffusion coefficient of oxidant X in the alloy.
D_X^{eff}	Effective diffusion coefficient of non-metallic constituent X in the alloy as defined by equation [24].
f	Volume or mass fraction of scale precipitate in the subscale region.
ΔG^o_{AX}, ΔG^o_{BX}	Free energies of formation of AX and BX respectively per mole of oxidant, X.
$\Delta G^o_{[2]}$	Free energy change of reaction [2].
K	Parabolic rate constant describing rate of thickening of surface scale.
K_1, K_2	Parabolic rate constants describing rate of recession of subscale/surface scale and alloy/subscale interfaces respectively.
N_A, N_B	Mole fractions of components A and B in the alloy respectively.
N_B^o	Bulk mole fraction of component B in the alloy.
N_{AX}, N_{BX}	Mole fractions of components AX and BX in the scale phase respectively.

$\bar{N}_{BX}$	Average mole fraction of BX in the surface scale.
N_X	Atomic fraction of non-metallic oxidant dissolved in the alloy phase.
N_X^I, N_X^{II}	Atomic fraction of X dissolved in the alloy at the subscale/surface scale and alloy/subscale interfaces respectively.
p	Ratio of cation diffusivities in the scale: the lesser stable cation (A) to that of the more stable cation (B).
R	Gas constant.
r	Ratio of number of moles of precipitated subscale to total number of moles of metallic constituents in the alloy.
T	Temperature.
t	Time.
u	Position co-ordinate in the surface scale measured from the subscale/surface scale interface.
u_s	Instantaneous thickness of surface scale.
V_{all}, V_{sc}	Molar volumes of alloy and scale phases respectively, assumed independent of composition.
X	Oxidant.
x	Position co-ordinate in the alloy measured from the original alloy surface.
x_1, x_2	Positions of subscale/surface scale and alloy/subscale interfaces respectively, measured from original alloy surface.
y	Dimensionless position in surface scale defined as u/u_s.
β	Defined by equation [10] as $\exp[-\frac{1}{RT}\Delta G^o_{BX}]$ and representing the stability of the more stable scale constituent.
γ_1, γ_2,	Dimensionless rate constants describing the rate of displacement of the subscale/surface scale and alloy/subscale interfaces respectively and defined in equation [29] as $\sqrt{K_1/2D_X^{eff}}$ and $\sqrt{K_2/2D_X^{eff}}$ respectively.

γ_X^o Henry's law activity coefficient for X dissolved in the alloy.

λ Time-independent position in the alloy, expressed as $x/\sqrt{t}$.

ζ Ratio of observable thickness of subscale zone to thickness of surface scale $(x_2 - x_1)/\mu_s$.

ϕ Ratio of cation vacancy concentrations in pure AX and BX at a given activity of X, representing the concentration dependence of cation diffusivities in the scale.

ν Oxidant activity dependence of the cation diffusivities.

Ω Defined by equation [9] as $\exp[-\frac{1}{RT}(\Delta G^o_{BX} - \Delta G^o_{AX}]$ and representing the relative stabilities of the two scale components.

1. INTRODUCTION

Significant progress has been made recently (Bastow, Whittle and Wood, 1977) in the quantitative analysis of alloy oxidation phenomena, particularly in systems where a single phase scale, but containing both alloy components, is formed. Wagner's (1969) original equations describing the simultaneous transport of two or more cations through a growing surface scale have been extended and solutions obtained which demonstrate the dependence of the cation concentration profiles within the scale, and the overall scaling rate, on the thermodynamic and transport properties of the system. These include the relative diffusion rates of the participating metals in the alloy and ions in the scale, the degree of selective oxidation of the appropriate alloy component, the overall growth rate of the scale, and the activity of the oxidizing environment.

Oxidation of binary alloys of Co, Fe, Mn and Ni with one another produces such a solid solution scale, since the isotopic oxides CoO, FeO, MnO and NiO all have a simple cubic NaCl structure and form solid solutions over their entire composition ranges. Thus, providing the oxidation is carried out within a temperature and oxygen pressure regime which precludes spinel formation, the oxidation of these binary alloys provides an ideal test of the diffusional model. A comparison between experimentally determined cation profiles in the scales formed on Ni-Co alloys and profiles calculated using independently measured diffusion data showed excellent agreement (Bastow, Whittle and Wood, 1976). Experimentally determined parabolic rate constants were also in close agreement with the calculated values. Less rigorous testing using not

completely independent data for the oxidation of Fe-Mn (Mayer and Smeltzer, 1972), Fe-Ni (Dalvi and Smeltzer, 1974), Fe-Co (Mayer and Smeltzer, 1974), Co-Ni (Narita and Nishida, 1975a) and for the sulfidation of Fe-Ni alloys (Narita and Nishida, 1975b) also contribute toward the validity of the model.

This model, however, ignores the possibility of forming a zone of subscale within the alloy beneath the surface scale and although, as will be shown later, this does not affect the validity of the original treatment in any way, for a full description of the scaling characteristics of this type of alloy it is necessary to analyze also the internal oxidation process. This is the purpose of the present paper and, since in essence the surface scale growth and the formation of internal oxide can be treated quite separately, reference to the former will only be included where absolutely necessary.

Internal oxidation in these systems is somewhat different from that classically reviewed by Rapp (1965), Swisher (1970), Meyering (1971) and others. They considered the formation of internal oxide in dilute alloys in which the solute metal forms a more stable oxide than the solvent metal oxide and in which oxygen has appreciable solubility in the solvent. Ag or Cu-base alloys containing small concentrations of a stable oxide forming element such as In, Al, Cr, Be, etc., are the prime examples. Thus, oxygen dissolves in the alloy at the alloy/surface scale interface at an activity corresponding to the equilibrium between the noble element oxide and the alloy, diffuses inwards and reacts with the base element to form its more stable oxide, within the alloy. Because the

concentration of the base element in the alloy is small, the oxide is precipitated as discrete particles rather than a continuous layer, and a zone consisting of a base metal denuded matrix and precipitated oxide grows inwards into the alloy. The two characteristic features of this type of internal oxidation are: the internal oxide is a different phase from the surface scale, and the concentration of internal oxide in the internal oxidation zone is approximately constant with depth below the surface.

Wagner (1968) pointed out that in certain circumstances it was possible to have the same oxide formed both as an external scale and as internal oxide precipitate within the alloy. Thus, when the oxidizing conditions favor the formation of the less noble metal as a surface scale then this will produce a depletion of this element in the alloy near the surface. If diffusion of oxygen into the alloy occurs, then, although the dissolved oxygen and less noble metal concentrations near to the interface may not be sufficient to cause oxide precipitation, they can be deeper in the alloy; the oxygen content will necessarily be lower, but the less noble metal content will be higher. Thus, the solubility product for oxide formation could well be exceeded leading to supersaturation of the alloy with respect to the oxide. Thus, formation of internal oxide in these systems stems from the depleted zone of the less noble component of the alloy below the surface scale. Wagner defined a limiting condition for the onset of an internal oxidation zone beneath the external scale based on the gradient of the solubility product at the alloy/scale interface. Smeltzer and Whittle (1978) expanded this analysis to account for the ternary interactions which

are very significant in systems such as those containing two metallic components with widely different affinities for oxygen, and dissolved oxygen. The ternary interactions have a strong influence on both the system thermodynamics, and the transport properties.

In contrast, then, to the previous, "classical", type of internal oxidation, in these latter systems the internal oxide is the same phase as the surface scale and, within the zone of internal oxidation, its concentration varies with position. The internal oxidation of alloys forming solid solution scales also fall into this latter category: the internal oxide is the same phase as the surface scale, although differing in composition, and, as will be demonstrated, its amount varies through the zone of internal oxidation. However, since the affinities of the alloy components for oxygen are similar, ternary interaction of the type indicated above will not be of great significance, and can be ignored.

In the analysis which follows, the completely general case of a binary alloy reacting with an oxidant X is considered, where the oxidant could be oxygen, sulfur or carbon. Indeed, the analysis is probably well suited to internal carbide precipitation. Unlike oxides, with the exception of the cubic oxides referred to earlier, many of the common metal carbides are intermiscible and thus when an alloy is exposed to a carbon-containing atmosphere, internal carburization takes place forming carbide precipitates of variable composition. In general, surface carbide layers are seldom observed. This phenomenon of degradation by internal carburization is rapidly increasing in significance in many studies relating to the degradation of materials in coal

conversion and petrochemical processing systems, and it is planned to apply the analysis to this type of corrosive attack. This may well prove to be more fruitful since more data are available on the thermodynamics and transport properties in alloy-carbon systems.

2. THEORY

(a) Oxidation Model

The system being considered is one in which an initially homogeneous, binary alloy, A-B, is oxidized by a single oxidant, X, and a scale consisting of a solid solution of the compounds AX and BX is formed. In addition, the oxidant X can dissolve in the alloy, diffuse inwards and cause internal precipitation of scale, which again consists of the solid solution AX-BX. The concentration of internally precipitated scale is sufficiently small that the cross-sectional area of the metallic matrix available for the inward diffusion of the oxidant is not reduced. In addition, it is assumed that there are no preferential paths for inward diffusion of the oxidant, such as alloy grain boundaries, or along the interfaces between the oxide particles and the matrix. [This latter phenomenon has not been generally recognized although recent evidence (Shida et al. 1979) suggests it may be critical in some systems: not, however, of the type considered here.] These two effects, the blocking of the inward diffusion of oxidant by the precipitates, and its enhancement along the precipitate/matrix interface, will of course tend to cancel each other out.

It is also assumed that diffusion control is maintained at all stages of the reaction. Nucleation of the surface scale and of the internal

precipitates is assumed to be instantaneous, interface compositions are assumed to take their equilibrium values throughout and any transient effects arising because of deviations from these conditions are assumed to have a negligible influence on the progress of the reaction.

Figure 1 shows schematically the diffusion profiles which develop in the alloy, scale and internal subscale regions, and the co-ordinate systems used in the description of the diffusion processes. The co-ordinate frames of x and λ have their origins at the original alloy surface and $\lambda = x/\sqrt{t}$. The frames of u and y have origins at the alloy/surface scale interface and $y = u/u_s$ where u_s is the instantaneous surface scale thickness. The use of parametric co-ordinates λ and y results in profiles which are invariant with time t. The surface scale is assumed to grow solely by the outward diffusion of cations and electrons resulting in a displacement of the alloy/surface scale interface inwards. The position, x_1 at time t, relative to the original surface of the alloy can thus be set as

$$x_1 = \sqrt{2K_1 t} \qquad [1]$$

where K_1 is the so-called corrosion constant defined by Wagner (1952). Further considerations of the growth of the surface scale are not included here, but may be found in the earlier references. The co-ordinate systems u and y are only included in Figure 1 for completeness.

(b) Alloy-Oxidant Phase Diagram

The internal oxidation process can best be visualized by reference to an isothermal section of the phase diagram which shows oxidant activity as a function of composition. As indicated earlier, both

alloy and scale phases show complete solid solubility and, as a limiting case, it may be assumed that both solutions exhibit thermodynamically ideal behavior. Then, considering the reaction

$$AX(\text{scale soln.}) + B(\text{alloy soln.}) = A(\text{alloy soln.}) + BX(\text{scale soln.}) \quad [2]$$

which has a standard Gibbs free energy change

$$\Delta G^{o}_{[2]} = \Delta G^{o}_{BX} - \Delta G^{o}_{AX} \quad [3]$$

where ΔG^{o}_{AX} and ΔG^{o}_{BX} are the Gibbs standard free energies of formation of pure compounds AX and BX respectively, and thus

$$\frac{N_A}{N_B} \cdot \frac{N_{BX}}{N_{AX}} = \exp\left[-\frac{1}{RT}\Delta G^{o}_{[2]}\right] = \exp\left[-\frac{1}{RT}(\Delta G^{o}_{BX} - \Delta G^{o}_{AX})\right] \quad [4]$$

with N_A, N_B, N_{AX} and N_{BX} representing the mole fractions of A, B, AX and BX in the alloy and scale phases respectively. Combining this with a similar expression for the reaction

$$B(\text{alloy soln.}) + 1/2X_2(g) = BX(\text{scale soln.}) \quad [5]$$

with

$$\frac{N_{BX}}{N_B \cdot a_X} = \exp\left[-\frac{1}{RT}\Delta G^{o}_{BX}\right] \quad [6]$$

enables the alloy and scale compositions to be obtained as a function of the oxidant activity. Thus, since

$$N_A = 1 - N_B \qquad \text{and} \qquad N_{AX} = 1 - N_{BX} \quad [7]$$

$$N_B = \frac{\frac{\Omega}{\beta a_X} - 1}{\Omega - 1}$$

and $$N_{BX} = \frac{\Omega - \beta a_X}{\Omega - 1} \qquad [8]$$

where $$\Omega = \exp\left[-\frac{1}{RT}\left(\Delta G^{o}_{BX} - \Delta G^{o}_{AX}\right)\right] \qquad [9]$$

and $$\beta = \exp\left[-\frac{1}{RT}\Delta G^{o}_{BX}\right] \qquad [10]$$

Figure 2 shows an isothermal section of the A-B-X phase diagram for typical values of Ω (=5) and β ($=10^5$) as justified later. The value of Ω is in effect a measure of the difference in stabilities of the scale components AX and BX, and determines the slope of the boundary dividing the scale phase field and the two phase field, scale + alloy; β is the stability of the more stable compound (here assumed to be BX) and fixes the positions of phase fields on the a_X-axis. Larger values of Ω, the relative stabilities of the two scale components, would increase the slope of the boundary dividing the scale phase field and the two phase field, and larger values of β, the stability of the more stable scale constituent would move the entire phase diagram to lower oxidant activities.

Combining together equations [7] and [8] relates the scale and alloy compositions at equilibrium

$$N_{BX} = \frac{1}{1 + \frac{1}{\Omega}\left(\frac{1}{N_B} - 1\right)} \qquad [11]$$

(c) Diffusion Path

Consider initially the growth of the surface scale. As explained in an earlier paper (Bastow et al., 1977) the overall composition of the scale depends on the ratio of diffusion rates of metals in the alloy and

metallic ions in the scale, which can be conveniently represented by the ratio K_l/D_{all}, where K_l was defined earlier in equation [1] and is the parabolic rate constant for surface scale growth in terms of the displacement of the alloy/surface scale interface (effectively a measure of ionic diffusivity in the scale); D_{all} is the interdiffusion coefficient of the alloy. Two limiting cases were distinguished:

(1) When diffusion in the alloy is infinitely fast compared with that in the scale, $K_l/D_{all} \to 0$, and there is no concentration change in the alloy. In this case, the diffusion path for an alloy of initial composition a is shown schematically in Figure 3(i). The composition at the alloy surface, b, is identical to that in the bulk alloy, and this is in equilibrium with a scale of composition e. The diffusion path continues in the scale along either cd or cd' depending on whether B ions in the scale have a slower or faster diffusion rate than A ions. [The apparent mass imbalance evident in Figure 3(i) is because of the unreal assumption of an infinitely fast alloy interdiffusion rate: this also implies an infinite supply of the components.] Of course there is no possibility of internal oxidation under these conditions.

(2) When diffusion in the alloy is very slow in comparison with that in the scale, $K_l/D_{all} \to \infty$, then the overall ratio of A to B in the scale can be shown identical with that in the alloy (Whittle et al., 1975); that is, $\bar{N}_{BX} = N_B^o$, where $\bar{N}_{BX}$ is the average mole fraction of B(X) in the scale and N_B^o the bulk mole fraction of B in the alloy. The systems referred to earlier, namely Co, Fe, Mn and Ni alloys, fall within this category. Although the average scale composition is the same as that of the bulk alloy, the scale composition of the alloy/surface scale interface is greater or smaller than the average composition depending on

whether the ions of the component with the higher affinity for oxygen (B in the example) has a lower or higher diffusivity in the scale (Bastow et al., 1977): points d and f on the schematic diffusion paths in Figures 3(ii) and (iii) respectively. The continuation of the diffusion path in the surface scale follows to f and g respectively (the points at which a_X is equal to the value in the external atmosphere) making the average composition of the scale identical with the bulk composition of the alloy as demanded above. Consider now the remainder of the diffusion path where it passes from the surface scale to the alloy and consider firstly that shown in Figure 3(ii) for the case where the component with the higher affinity for the oxidant has the lower diffusivity in the scale. The scale composition, d, is in equilibrium with the alloy of composition e and if the oxidant diffused into the alloy at only a slow rate and its presence in the alloy could be disregarded, then the diffusion path would continue along the line eba, with the portion eb representing a negligible distance in real space (recall that in representing the diffusion path on an isothermal section of a phase diagram in this way, space and time coordinates disappear). Thus there would be a very narrow depletion zone of component B near to the alloy/surface scale interface: of course as the ratio K_l/D_{all} decreases, the depletion zone widens and the composition of the alloy at the interface with the surface scale, point e, moves down the alloy/alloy + scale boundary.

However, this is generally not the complete picture: the diffusivity of the oxidant in the alloy, D_X, is normally expected to be several orders of magnitude larger than D_{all}, since it diffuses as an interstitial,

rather than substitutionally. Thus, the diffusion path can cut into the two-phase field alloy + scale. As D_{all} is usually very small relative to D_X, there is no diffusion of the alloy components normal to the alloy/scale interface and the diffusion path within the two phase field is a virtual one and takes the right angled shape ecb. Thus, the length ec, an iso-potential line for oxygen, represents zero distance, and length cb a region of supersaturation where internal precipitation can be expected. This latter corresponds to the zone of internal subscale and the ratio of metallic constituents in this subscale zone remains equal to N_B^o. This is why, as indicated earlier, analysis of the concentration profiles within the surface scale (Bastow et al., 1976, 1977) is independent of whether a subscale is formed or not. In both cases, the ratio of alloying components entering the surface scale is identical to that in the bulk alloy. The composition of the alloy phase in the subscale zone follows the alloy/alloy + scale phase boundary, eb, and that of the subscale, the scale/alloy + scale boundary, db', making ecb a true composite diffusion path (Roper and Whittle, 1980), which thus also indicates the relative amounts of the two phases, alloy and precipitated scale in the subscale region. Of course, the segregation of the element with the higher affinity for the oxidant, B in this case, into the subscale implies that lateral diffusion, parallel to the surface scale interface, does occur. However, the distances over which this occurs, particularly if the precipitated phase is very finely divided, are very small in comparison to the thickness of the subscale zone and this does not conflict with the earlier assumption that there is no overall change in composition within the subscale zone. The complete path then is abcdf, and this can be calculated, and the fraction of

precipitated scale in the alloy at the subscale/surface scale interface determined unequivocally.

However, in the alternative case where the component which has the higher affinity for the oxidant also diffuses faster in the scale, this is not possible. The surface scale composition at the alloy/surface scale interface, f, and which is in equilibrium with alloy of composition, e, is to the left of the bulk alloy composition. Thus, allowing that if $D_X >> D_{all}$ as before, and that the continuation of the diffusion path towards the alloy adopts a right-angle shape, it would be unrealistic if it were to continue directly from point e in this manner: it would cut right across the two-phase alloy + scale field and into the single phase scale field. Thus, it seems clear that the path must first pass down the alloy/alloy + scale boundary before cutting into the two phase region. It follows edcba, with the portion of the diffusion path, ed, representing a thin band of alloy phase separating the surface scale from the subscale zone. The precise reason for this is not entirely clear, but it is observed experimentally (Gesmundo, Nanni, and Whittle, 1979; Shida et al., 1980). At sites further into the alloy the activity of oxidant, though decreasing, becomes sufficient to form a subscale. This situation is assisted by a steep concentration gradient of B and a flat activity gradient of X, as implied by the condition $D_X >> D_{all}$. The portion of the path dcb is thus similar to the portion ecb in Figure 3(ii), except that the exact location of point d, which gives the maximum fraction of precipitated subscale, cannot be defined in this case.

Again, if there were no diffusion of the oxidant in the alloy, the path would follow eba with the length eb representing virtually zero distance as discussed for Figure 3(ii).

(d) Transport Equations

Considering now the transport of the oxidant inwards from the alloy surface within the subscale region, which is supposed to reach a depth x_2 at time t measured from the original surface of the alloy, as shown in Figure 1. The alloy/surface scale interface at time t is at position x_1. An expression analogous to equation [1] which relates x_1 with t can be written for x_2:

$$x_2 = \sqrt{2K_2 t} \qquad [14]$$

where K_2 is a parabolic rate constant describing the growth of the subscale zone. In the subscale zone, the total amount of oxidant per mole of alloy is $N_X + \nu r$, where r is the ratio of the number of moles of precipitated scale to the number of moles of the metallic constituents of the alloy, ν is the number of moles of X per mole of scale, and N_X is the number of moles of X per mole of metallic constituents. Thus, ignoring any ternary interactions, which will be small in these types of systems for the reasons given earlier, and assuming that the amount of subscale is small so that volume changes and blockage of the diffusion path by the precipitate can be neglected, the rate of change in the total amount of X per mole of alloy at position x is given by

$$\frac{\partial}{\partial t}(N_X + \nu r) = D_X \frac{\partial^2 N_X}{\partial x^2} \qquad x_1 \leq x \leq x_2 \qquad [15]$$

This can be re-arranged to give

$$\frac{\partial N_X}{\partial t} = \frac{D_X}{1 + \frac{\nu \partial r}{\partial N_X}} \frac{\partial^2 N_X}{\partial x^2} \qquad x_1 \leqslant x \leqslant x_2 \qquad [16]$$

Assuming that the dissolution of the oxidant in the alloy follows Henry's law which is consistent with the lack of ternary interaction, as indicated above and earlier, then

$$N_X = a_X / \gamma_X^o \qquad [17]$$

and phase diagrams with N_X replacing a_X can be constructed from the previous diagrams. Figure 4 shows an enlarged version of the part of Figure 3 where the composite diffusion path crosses the two-phase field, with the relevant nomenclature. Thus, at any oxidant potential within the subscale zone, alloy of composition N_B is in equilibrium with scale particles of composition N_{BX}. Furthermore, since the overall composition in terms of metallic components in this two phase region is identical to that of the bulk alloy (i.e. there has been no diffusion of metal in or out of this zone) the mass fraction, f, of the scale (or volume fraction if volume changes are neglected) is given by the lever rule

$$f = \frac{N_B - N_B^o}{N_B - N_{BX}} \qquad [18]$$

where N_B^o is the mole fraction of B in the bulk alloy. r, the ratio of number of moles of precipitated scale to the number of moles of the metallic constituents of the alloy, as used in equations [15] and [16], is related to f by

$$r = \frac{f}{1-f} \qquad [19]$$

Thus, f can vary from 0 to 1, although for reasons given later probably does not exceed 0.3; the corresponding variation of r would be from 0 to ∞, with 0.429 corresponding to a value of f = 0.3.

Thus, combining equations [18] and [19] gives

$$r = \frac{N_B - N_B^o}{N_B^o - N_{BX}} \qquad [20]$$

According to the expressions given earlier, both N_B and N_{BX} can be expressed as functions of a_X, equations [7] and [8] and thus as functions of N_X through equation [17]. Thus,

$$r = \frac{\frac{\Omega}{\beta a_X} - 1 - N_B^o(\Omega-1)}{(\Omega-1)N_B^o - \Omega + \beta a_X} \qquad [21]$$

$$r = \frac{\frac{\Omega}{\beta\gamma_X^o N_X} - 1 - N_B^o(\Omega-1)}{(\Omega-1)N_B^o - \Omega + \beta\gamma_X^o N_X} \qquad [22]$$

The ratio of subscale particles to metallic constituents in the alloy, r, is plotted as a function of a_X in Figure 5 using the values of Ω and β used to construct the phase diagram in Figure 1. Up to ratios of subscale particles to metallic constituents in the alloy of 0.3 the relationship is virtually linear: indeed if data points are calculated at intervals of r of 0.05, the correlation coefficient for a least mean squares fit

of r and a_X is extremely close to 1, as shown in the table.

The gradient, $\partial r/\partial a_X$, increases as the bulk mole fraction of B in the alloy increases; this is related to the change in slope of the phase boundary separating the alloy and alloy + scale regions in the phase diagram. Thus, since $\partial r/\partial a_X$ and hence $\partial r/\partial N_X$ are essentially constant, equation [16] may be re-written as

$$\frac{\partial N_X}{\partial t} = D_X^{eff} \frac{\partial^2 N_X}{\partial x^2} \qquad x_1 \leq x \leq x_2 \qquad [23]$$

where the effective diffusion coefficient is given by

$$D_X^{eff} = \frac{D_X}{1 + \nu \frac{\partial r}{\partial N_X}} \qquad [24]$$

Equation [23] now has a normal error function solution:

$$N_X = N_X^I - (N_X^I - N_X^{II}) \frac{\operatorname{erfc} \frac{x}{2\sqrt{D_X^{eff} t}} - \operatorname{erfc} \frac{x_1}{2\sqrt{D_X^{eff} t}}}{\operatorname{erfc} \frac{x_2}{2\sqrt{D_X^{eff} t}} - \operatorname{erfc} \frac{x_1}{2\sqrt{D_X^{eff} t}}} \qquad [25]$$

Diffusion of the oxidant ahead of the alloy/subscale interface, $x > x_2$ follows the conventional transport equation and thus

$$N_X = N_X^{II} \frac{\operatorname{erfc} \frac{x}{2\sqrt{D_X t}}}{\operatorname{erfc} \frac{x_2}{2\sqrt{D_X t}}} \qquad [26]$$

and equating the fluxes at $x = x_2$

$$\lim_{\delta \to 0} \quad D_X \frac{\partial N_X}{\partial x} \Big| x = x_2 - \delta = D_X \frac{\partial N_X}{\partial x} \Big| x = x_2 + \delta \qquad [27]$$

Since there is no subscale formation at x_2, using equations [25] and [26] to substitute into [27], gives a transcendental equation for x_2

$$\frac{N_X^I - N_X^{II}}{N_X^{II}} \sqrt{1 + \nu \left|\frac{\partial r}{\partial N_X}\right|} = \exp \left[\frac{\nu \gamma_2^2 \left|\frac{\partial r}{\partial N_X}\right|}{1 + \nu \frac{\partial r}{\partial N_X}} \right] \frac{\operatorname{erfc} \gamma_1 - \operatorname{erfc} \gamma_2}{\operatorname{erfc} \frac{\gamma 2}{\sqrt{1 + \nu \frac{\partial r}{\partial N_X}}}} \qquad [28]$$

where $\gamma_1 = \frac{x_1}{2\sqrt{D_X^{eff} t}} = \sqrt{\frac{K_1}{2D_X^{eff}}}$ and $\gamma_2 = \frac{x_2}{2\sqrt{D_X^{eff} t}} = \sqrt{\frac{K_2}{2D_X^{eff}}}$ [29]

Thus, solution of equation [28] gives γ_2 and hence K_2, the rate of subscale penetration, and solution of equation [25] gives the profile of dissolved oxidant throughout the subscale zone. Use of equations [20], [7] and [8] then permit the fraction of subscale, composition of the

alloy, and the composition of the subscale respectively to be calculated throughout the subscale region.

The actual observable depth of subscale would be given by

$$x_2 - x_1 = \sqrt{2t}\ (\sqrt{K_2} - \sqrt{K_1}) = 2\sqrt{\frac{D_X t}{1 + \nu \frac{\partial r}{\partial N_X}}}\ [\gamma_2 - \gamma_1] \qquad [30]$$

However, as indicated earlier, except possibly in cases where the alloy component with the highest affinity for the oxidant is the slower diffusing species in the scale, it is not possible to fix a priori the value of r, the ratio of number of moles of precipitated subscale to the moles of alloy components, at the subscale/surface scale interface. As a consequence, the following calculations have been carried out by assuming different values of r_1, the value of r at the subscale/surface scale interface, and the dependence of the observable depth of subscale, $x_2 - x_1$, on r_1, and the other important parameters, examined. Assigning a value to r_1 in turn fixes a_X^I or N_X^I, the activity or atom fraction of the oxidant at this interface, which is also the point at which the diffusion path cuts into the two phase alloy + scale region. Generally, r_1 is not expected to exceed 0.3, since in studies of internal oxidation this value marks the transition from internal oxidation to exclusive external scale formation (Rapp, 1965).

3. TYPICAL DATA

The following parameters are important in determining the extent and composition of the subscale:

Ω, the relative stabilities of the two scale components

β, the stability of the more stable scale constituent

N_B^o, the bulk alloy composition

D_X, the diffusivity of the oxidant in the alloy

K_1, the growth rate constant of the surface scale

Values of Ω are typically in the range 5-1,000 for binary alloys containing Co, Fe and Ni at 1273 K, but can be as high as 10^6 at this temperature for alloys containing Mn. Table I lists the standard free energies of formation of the four cubic oxides CoO, FeO, MnO and NiO at 1273 K. Thus, values of 5, 10, 50, 100 and 1,000 for Ω, which have been used in the calculations, correspond to differences in free energies of formation of the scale components of 17094, 24456, 41551, 48680, and 73020 J (4070, 5823, 9893, 11646 and 17469 cal.) respectively at 1273 K. Similarly, as in Table I, β has a value in the range 10^5 - 10^8 for CoO, FeO and NiO extending to 10^{12} for MnO at 1273 K. Values in the range of 10^5 - 10^8 have been used in the calculations, which correspond to -122,281 to -195,650 J (-29,115 to - 46,583 cal.) for the standard free energy of formation of the more stable oxide at 1273 K.

Few data are available for D_X, the diffusivity of the oxidant in these metals. Table II summarizes those available in Diffusion Data. Typical values lie in the range 10^{-8} - 10^{-6} cm^2/s, although, as indicated earlier, the apparent diffusivities may be somewhat higher in the presence of an internal oxide precipitate.

The growth rate of the surface scale depends on alloy composition. According to the earlier analysis (Bastow et al., 1976), the parabolic

scaling rate constant in terms of scale thickness, K, for the growth of these solid solution surface scales AX - BX depends on the cation concentration profiles developed in the scale. However, to a good approximation

$$K = \nu\, D_B^o\, \phi^{\bar{N}_{BX}-1}\, [p + (1-p)\bar{N}_{BX}]\, [(a_X'')^{1/\nu} - (a_X')^{1/\nu}] \qquad [31]$$

where ν is the oxidant activity dependence of the cation diffusivity, D_B^o is the self-diffusion coefficient of B cations in pure BX at unit activity of X, ϕ (denoted β in the original paper but changed here to avoid confusion) is the ratio of cation vacancy concentrations in pure AX and pure BX at a given activity of X, and represents the concentration dependence of cation diffusivities in the scale; $\bar{N}_{BX}$ is the average mole fraction of BX in the scale, which as indicated earlier under these conditions is identical to N_B^o, p is the ratio of cation diffusivities in the scale (D_A/D_B) and a_X'' and a_x' are the activities of X at the outer and inner interfaces of the surface scale.

However, in the present analysis, rather than use equation [31] to calculate the rate constant K, which would necessitate assigning values to the constants D_B^o, ν, ϕ and p, all that is required is the variation of K with alloy composition, N_B^o: or average scale composition, $\bar{N}_{BX}$, since the two are identical. Thus, differentiating equation [31] gives

$$\frac{d \ln K}{d\bar{N}_{BX}} = \frac{d \ln K}{dN_B^o} = \ln \phi + \frac{1-p}{p + (1-p)\bar{N}_{BX}} \qquad [32]$$

which if p is not very different from unity may be approximated to

$$\frac{d \ln K}{dN_B^o} \simeq \text{const.} \qquad [33]$$

Thus, relating K_1, the rate constant in terms of the displacement of the alloy/surface scale interface as defined in equation [1] with K the rate constant in terms of scale thickness gives

$$K_1 = (1-N_B^o)\ K_1(A) + N_B^o\ K_1(B) \qquad [34]$$

where $K_1(A)$ and $K_1(B)$ are the values of K_1 for pure components A and B respectively. Typical ranges of values are 10^{-12} - 10^{-9} cm^2/s.

4. CALCULATED RESULTS AND DISCUSSION

(a) Typical Concentration Profiles

Figure 6 shows typical profiles through the subscale zone, which extends from $x_1/\sqrt{t}$ to $x_2/\sqrt{t}$, of the ratio of moles of subscale to the number of moles of metallic components in the alloy, the composition of the subscale, the composition of the alloy, and the concentration of dissolved oxidant. As indicated earlier, the subscale contains a higher concentration of the selectively oxidized component, B, in the current example, at deeper depths below the surface, but the fraction of subscale falls off dramatically. Values of the various parameters are given in the caption: in Figure 6(a) the subscale ratio at the surface scale/subscale interface was taken as 0.1, whilst it had a value of 0.3 in Figure 6(b). Clearly, as reference to the phase diagram, Figure 2, indicates, this also corresponds to a lower B content in the alloy phase and a lower BX content in the subscale at the surface scale/subscale interface. The depth of subscale is also greater when the fraction

of subscale at the interface with the surface scale is higher. At the alloy/subscale interface, the alloy composition is identical to that of the bulk alloy, as explained earlier; the dissolved oxidant concentration profile is very flat within the subscale-free zone since the effective diffusivity of the oxidant in this zone is orders of magnitude greater than its effective diffusivity in the subscale zone.

(b) Variation of Subscale Depth with Alloy Composition

As indicated in equation [30] the observable depth of subscale formation is given by $(x_2 - x_1)$ or $(x_2 - x_1)/\sqrt{t}$ to remove the time dependency. It seems more appropriate, however, to express this as a ratio to the surface scale thickness, u_s, and this is denoted by ξ where

$$\xi = \frac{x_2 - x_1}{u_s} = \frac{x_2 - x_1}{x_1} \frac{V_{all}}{V_{sc}} \qquad [35]$$

where V_{all} and V_{sc} are the molar volumes of the alloy and scale respectively, and the scale has an anion to cation ratio of unity. V_{all}/V_{sc} has a value of around 2 in typical systems, and this is the value which has been used.

The ratio of subscale/surface scale thickness, ξ, is shown as a function of alloy composition for various values of r_1, the maximum concentration of subscale at the subscale/surface scale interface, which has to be chosen arbitrarily in most cases, in Figure 7: the other parameters are indicated in the caption. The subscale/surface scale ratio increases sharply initially with increasing concentration of B, the selectively oxidized element in the alloy, and then decreases slowly with the maximum occurring at around $N_B^o = 0.1 - 0.2$. This is related

to two factors: firstly, the position of the diffusion path on the ternary phase diagram where with alloys more dilute in B the path lies close to the steeper regions of the oxidant solubility curve, and secondly the width of the two phase region alloy + scale on the phase diagram which goes through a maximum for an alloy of around about $N_B = 0.3$.

Interestingly, the depth of subscale is not a strong function of the fraction of subscale at the surface scale/subscale interface; this latter parameter also fixes the concentration of the dissolved oxidant in the alloy as indicated on the phase diagram.

The variation of position of the subscale/surface scale interface, x_1, is also dependent on alloy composition, increasing or decreasing with increasing B concentration in the alloy, depending on whether B cations or A cations diffuse faster in the scale.

(c) Variation of Subscale Depth and the Concentration Profiles With Oxide Stability

Figure 8 shows the variation of the subscale/surface scale ratio with alloy composition for different values of Ω and β which are the measures of the oxide stability. Recall that Ω is essentially the difference in stabilities of the two scale components and determines the slope of the boundary between scale and scale + alloy fields on the phase diagram. Increase in Ω, which increases the slope and corresponds to a greater difference in stability between the scale components, has a strong influence on the depth of subscale penetration. Increase in Ω also causes the maximum value of subscale/surface scale thickness ratio to occur at smaller values of N_B^O.

β, which is a measure of the stability of the more stable scale component has a lesser influence on the depth of subscale penetration. This effect is opposite to that of Ω in that the larger the value of β, the smaller is the subscale penetration, and this is related to the lower overall solubility of the oxidant in the alloy. Indeed, if the difference in oxygen activities between the surface scale/subscale and subscale/alloy interfaces, a_o^I and a_O^{II} respectively is calculated for different alloy compositions, then for a given fraction of subscale at the subscale/surface scale interface, this shows a similar dependence on N_B^o as does ξ, the subscale/surface scale thickness ratio. Furthermore, for different values of Ω and β the positions of the maxima in the ξ/N_B^o curves are identical to those in the $(a_o^I - a_O^{II})$ curves, and it is probable that the thermodynamic factors alone control the variation of subscale depth with alloy composition.

Figure 9 shows the various concentration profiles as a function of the thermodynamic variables Ω and β. Clearly when $\Omega = 50$ and there is a relatively large difference in stability between the scale components BX and AX, then the composition of the subscale is very rich in BX, and does not vary much with depth below the surface. As a consequence of the subscale being richer in BX, the alloy phase shows a greater depletion in component B.

(d) Effect of Oxidant Diffusivity

Figure 10 shows the subscale depth, $(x_2 - x_1)/\sqrt{t}$, rather than the surface scale/subscale thickness ratio as a function of alloy composition for a number of different diffusion coefficients of the oxidant in the range 10^{-8} to 10^{-5} cm^2/s. It is clear

that a decrease in D_X produces a strong decrease in the depth of the subscale penetration, when all the other parameters remain the same. It is, however, to be noted that the critical parameter is not only the absolute value of D_X, but also its value relative to the parabolic rate constant which describes the recession of the surface scale/subscale interface. This has a value in the range 10^{-12} - 10^{-10} cm^2/s (depending on alloy composition) for the data given in Figure 10, and thus it is clear that D_X/K_1 must be greater than about 10^4 before any significant depth of subscale is likely to be observed. Figure 11 shows the change of subscale depth with alloy composition for different values of the parabolic rate constant for the displacement of the surface scale/subscale interface, taking $K_1(A) = K_1(B)$ to avoid complications arising from the change in rate constant with alloy composition. Although an increase of K_1 produces a decrease of the subscale depth, the effect is not as large as that produced by a corresponding change of D_X. It is to be noted, however, that the effect is greater, the greater K_1. In particular, when K_1 becomes small, there is virtually no change in the depth of subscale and all the curves tend to coincide with that obtained in the absence of an external scale. This is because when K_1 is very small in comparison with D_X, the outer surface scale/subscale interface is virtually immobile with respect to the inner subscale/alloy interface, so that the depth of internal subscale depends only on the rate of penetration of the oxidant into the alloy. On the other hand, when K_1 is not negligible with respect to D_X, penetration of X into the alloy is faster because the surface scale/subscale interface, which is the source of the oxidant, encroaches more rapidly into the alloy. However,

this is compensated by a rapid conversion of the outer portion of the subscale region into surface scale, so that its effective thickness is reduced.

(e) Effect of Surface Scaling Rate

As indicated earlier, the parabolic growth rate of the surface scale on this type of alloy varies exponentially with the bulk alloy composition, providing p, the ratio of diffusivities in the scale of the lesser stable cation (A) to more stable cation (B), is not too different from 1. Furthermore, the rate constant can increase, or decrease, with increasing alloy content of the component with the greater affinity for the oxidant (B in the present example) depending on whether B or A cations are more mobile respectively in the solid solution scale.

The case where the rate constant for scale growth is independent of alloy composition has already been discussed in conjunction with the effect of D_X. The other data presented thus far relate to cases where the more stable cation is also the faster diffuser. Figure 12 compares the ratio of surface scale/subscale thickness as a function of alloy composition when the more stable cation is the faster and slower diffuser in the scale. Essentially there is no difference in behavior since although in the former case the growth rate of the surface scale increases with increasing B content in the alloy, whilst in the latter it decreases, this variation has been accounted for by calculating the surface scale/subscale thickness ratio.

5. CONCLUSIONS

The diffusion processes occurring when a binary alloy reacts with a simple oxidant to form both a surface scale and a subscale of the same phase, but differing in composition, have been analyzed. The concentration of subscale varies with depth below the subscale/surface scale interface and becomes richer in the more stable scale component. The variation in ratio of subscale/surface scale thickness depends primarily on the thermodynamic parameters of the system, namely the stabilities of the two scale components. Increase in the diffusivity of the oxidant also increases the depth of subscale penetration as might be expected. The rate of surface scale growth has only a minor effect.

REFERENCES

Barin, I. and Knacke, O. 1973, Thermodynamic Properties of Inorganic Substances, Springer-Verlag, Berlin.

Bastow, B. D., Whittle, D. P. and Wood, G. C. 1976, Corros. Sci. 16, 57-69.

Bastow, B. D., Whittle, D. P. and Wood, G. C. 1977, Proc. Roy. Soc. A 356, 177-214.

Dalvi, A. D. and Smeltzer, W. W. 1974, J. electrochem. Soc. 121, 386-394.

Gesmundo, F., Nanni, P., and Whittle, D. P. 1979, Corros. Sci. 19, 675-691.

Mayer, P. and Smeltzer, W. W. 1972, J. electrochem. Soc. 119, 626-631.

Mayer, P. and Smeltzer, W. W. 1974, J. electrochem. Soc. 121, 538-543.

Meyerling, J. L. 1971, Adv. in Materials Science 5, 1-81.

Narita, T. and Nishida, K. 1975a, Nippon Kink. Gakk. 29, 1152-1164 (English translation kindly provided by authors.)

Narita, T. and Nishida, K. 1975b, Denki Kagaku 43, 443-452.

Rapp, R. A. 1965, Corrosion 21, 382-397.

Roper, G. W. and Whittle, D. P. 1980, to be published.

Shida, Y., Wood, G. C., Whittle, D. P. and Stott, F. H. 1979, to be published.

Smeltzer, W. W. and Whittle, D. P. 1978, J. electrochem. Soc. 125, 1116-1126.

Swisher, J. H. 1971, Oxidation of Metals and Alloys, ed. D. L. Douglass, 235-248.

Wagner, C. 1952, J. electrochem. Soc. 99, 369-385.

Wagner, C. 1968, Corros. Sci. 8, 889-895.

Wagner, C. 1969, Corros. Sci. 9, 91-109.

Whittle, D. P., Bastow, B. D. and Wood, G. C. 1975, Oxid. Metals 9, 215-223.

TABLE I. Standard Free Energies of Oxide Formation at 1273 K.
(Barin and Knacke, 1973)

Oxide	ΔG^{o}	
	J	Cal.
CoO	-144,895	-34,664
FeO	-190,370	-45,543
MnO	-291,256	-69,678
NiO	-126,884	-30,355

TABLE II. Diffusivity of Oxygen in the Metal at 1273 K. (Diffusion Data)

	D_O, cm^2/s
Co	8.6×10^{-9}
Fe	6.8×10^{-7}
Mn	-
Ni	6.9×10^{-9}

FIGURE CAPTIONS

Figure 1. Schematic diagram of the oxidation model.

Figure 2. The alloy-scale phase diagram at 1273 K calculated with $\Omega = 5$ and $\beta = 10^5$.

Figure 3. Schematic diffusion paths:

(i) no subscale formation

(ii) subscale formation and component A the faster diffusing species in the scale

(iii) subscale formation and component B the faster diffusing species in the scale.

Figure 4. Enlarged schematic diffusion path on the phase diagram indicating nomenclature.

Figure 5. Fraction of subscale as a function of activity of oxidant in the alloy with $\Omega = 5$ and $\beta = 10^5$.

Figure 6. Calculated concentrations of BX in subscale, B and X in alloy and fraction of subscale as a function of position in the alloy.

$N_B^o = 0.4$; $\Omega = 5$; $\beta = 10^5$; $D_X = 10^{-5}$ cm^2/s;

$K_l(A) = 10^{-12}$ cm^2/s, $K_l(B) = 10^{-10}$ cm^2/s

(a) r at surface scale/subscale interface $\simeq$ 0.1

(b) r at surface scale/subscale interface $\simeq$ 0.3.

Figure 7. Subscale/surface scale thickness ratio as a function of alloy composition and fraction of subscale at surface scale/subscale interface.

$\Omega = 5$; $\beta = 10^5$; $D_X = 10^{-5}$ cm^2/s; $K_l(A) = 10^{-12}$ cm^2/s; $K_l(B) = 10^{-10}$ cm^2/s

Figure 8. Subscale/surface scale thickness ratio as a function of alloy composition and the thermodynamic parameters Ω and β.

$D_X = 10^{-5}$ cm^2/s; $K_l(A) = 10^{-12}$ cm^2/s; $K_l(B) = 10^{-10}$ cm^2/s; $r = 0.3$ at X_1

(a) $\beta = 10^5$; (b) $\Omega = 5$

Figure 9. Calculated concentrations of BX in subscale, B and X in alloy, and fraction of subscale as a function of position, and the thermodynamic parameter Ω.

$\beta = 10^5$; $D_X = 10^{-5}$ cm^2/s; $K_l(A) = 10^{-12}$ cm^2/s; $K_l(B) = 10^{-10}$ cm^2/s; $r = 0.3$ at X_1 $N_B^o = 0.4$

Figure 10. Observable subscale depth as a function of alloy composition and oxidant diffusivity in the alloy.

$\Omega = 5$; $\beta = 10^5$; $K_l(A) = 10^{-12}$ cm^2/s; $K_l(B) = 10^{-10}$ cm^2/s; $r = 0.3$ at X_1

Figure 11. Observable subscale depth as a function of alloy composition and surface scale growth rate.

$\Omega = 5$; $\beta = 10^5$; $K_1(A) = K_1(B)$; $D_X = 10^{-5}$ cm^2/s; r = 0.3 at X_1

Figure 12. Subscale/surface scale ratio as a function of alloy composition and surface scale growth rate.

$\Omega = 5$; $\beta = 10^5$; $D_X = 10^{-5}$ cm^2/s; r = 0.3 at X_1

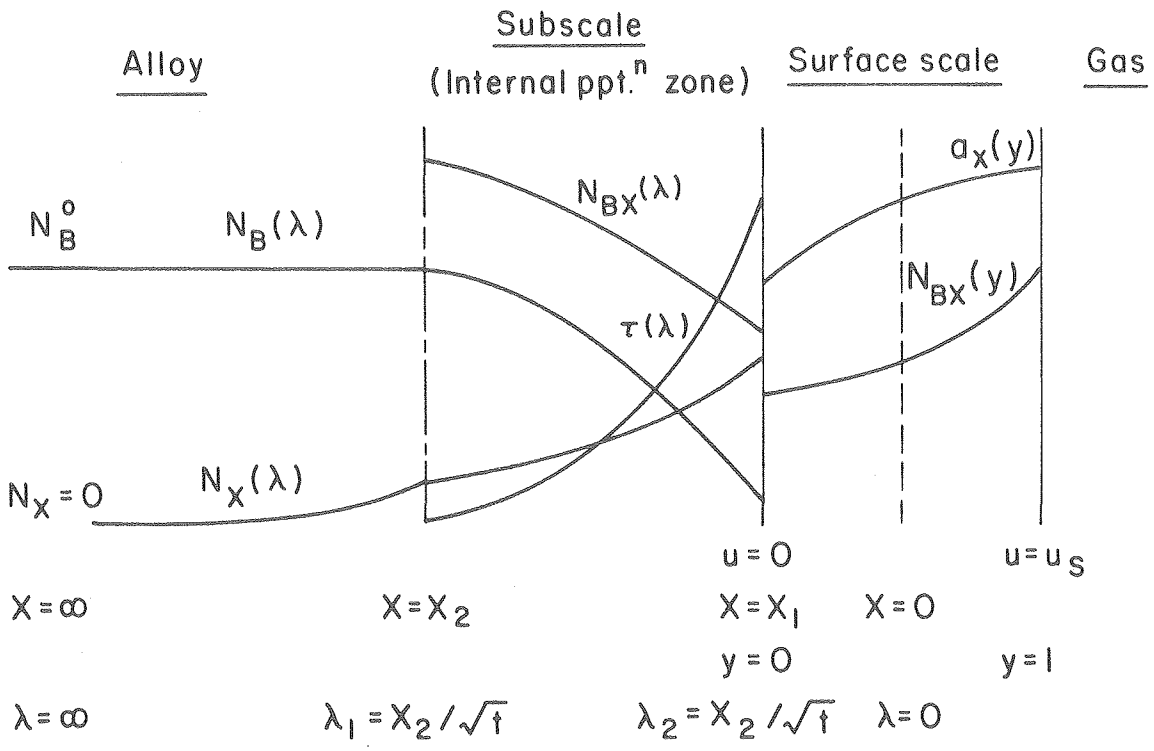

XBL 7911-13261

Figure 1

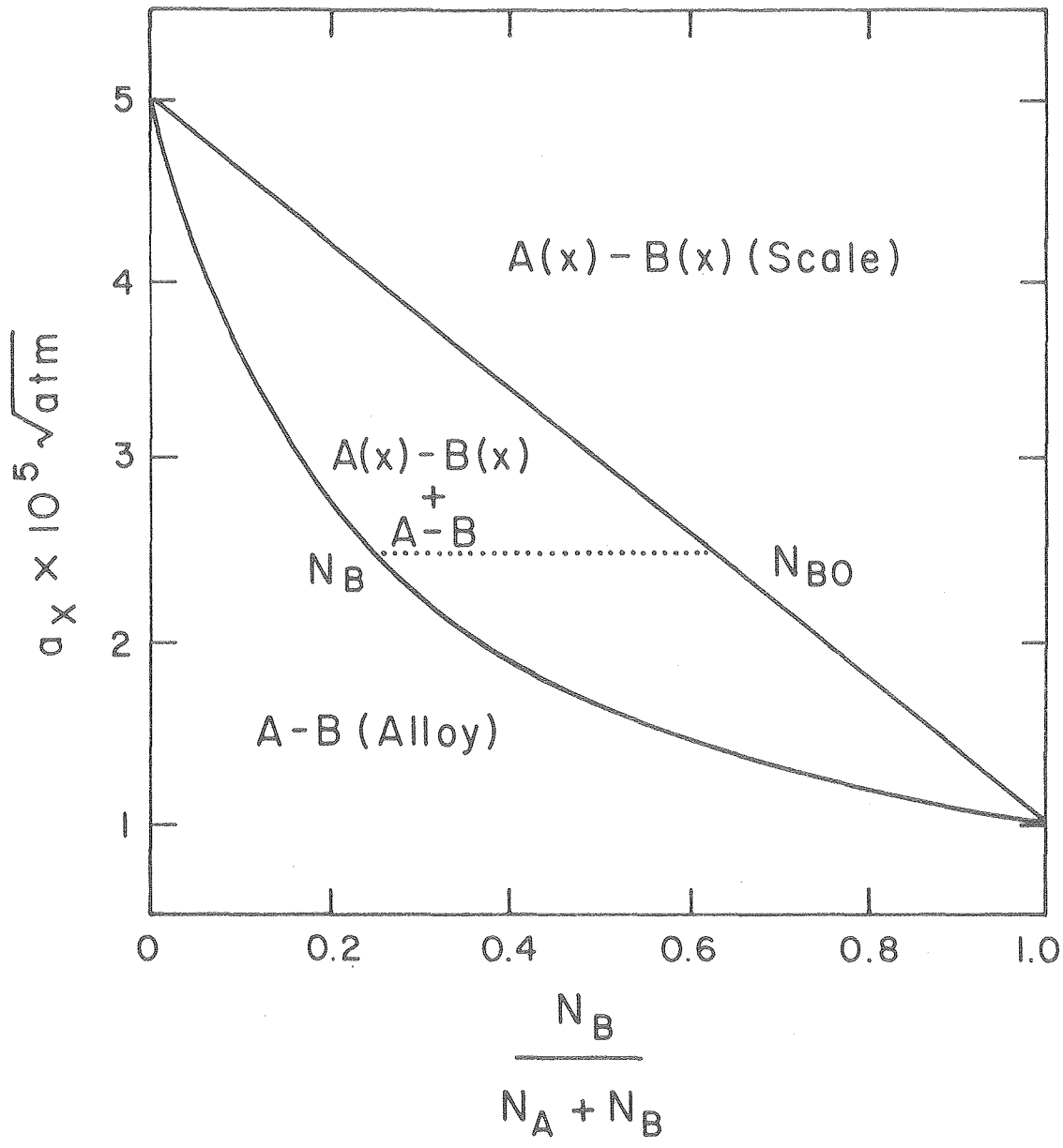

Figure 2

XBL 7911 - 13262

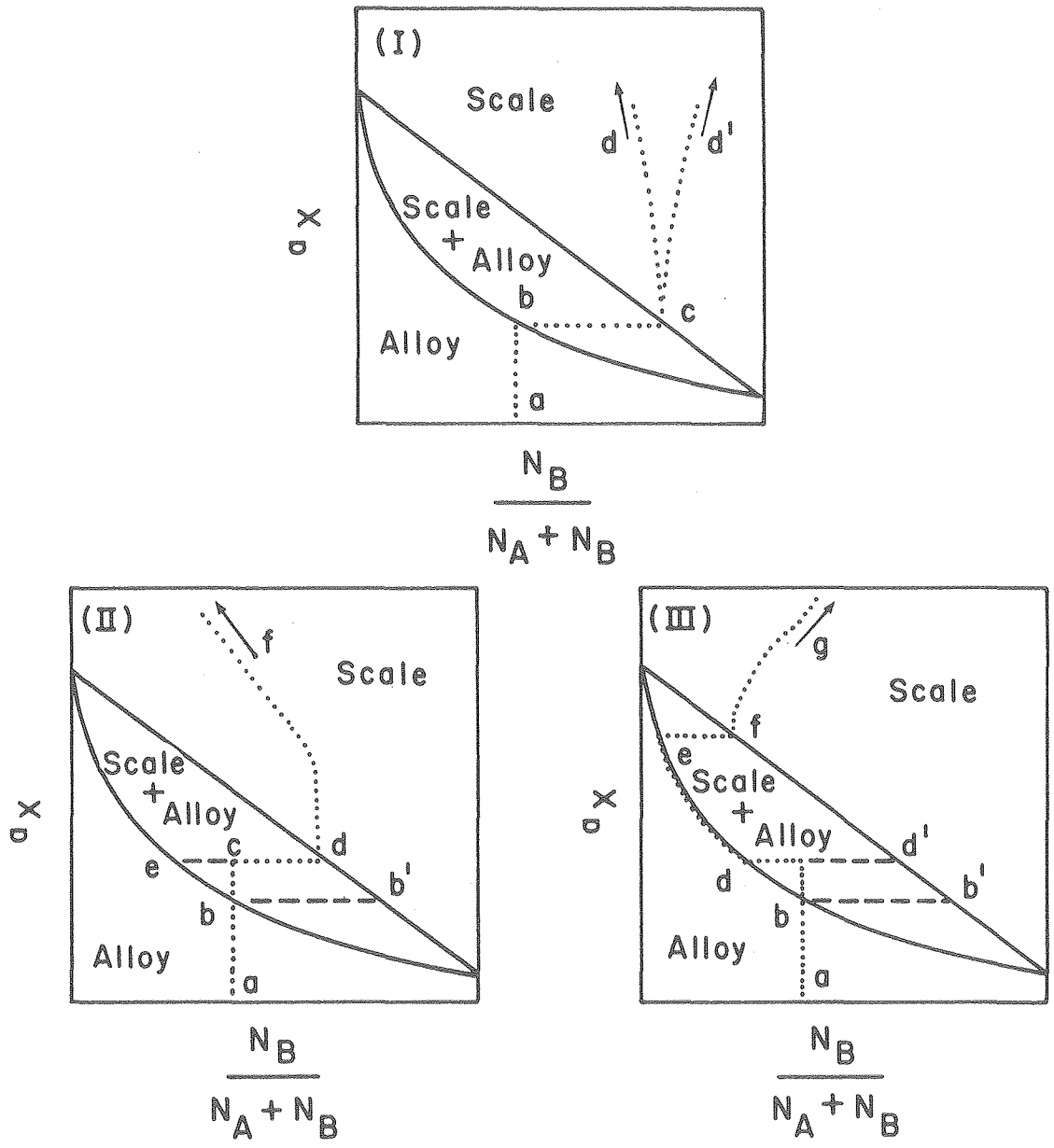

Figure 3

XBL 7911-13263

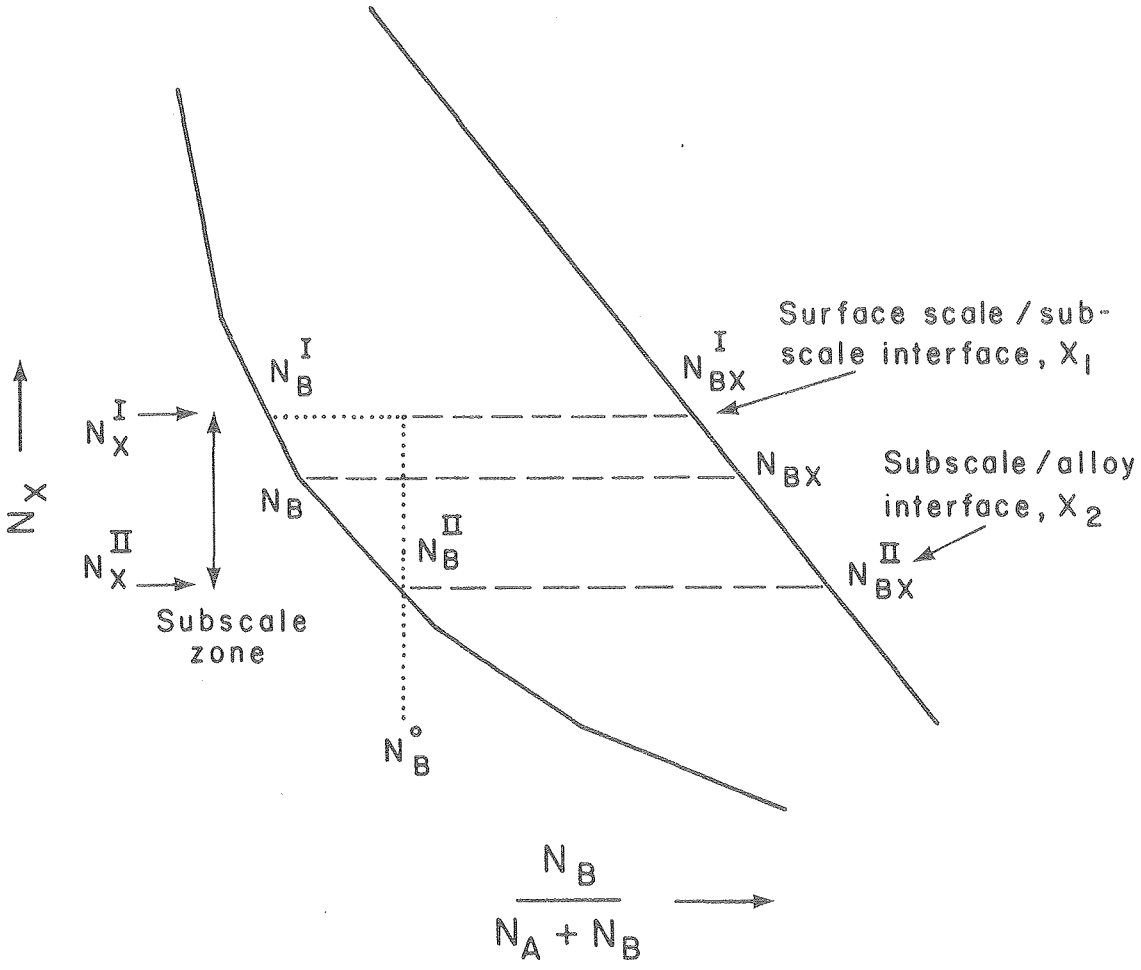

Figure 4

XBL 7911-13265

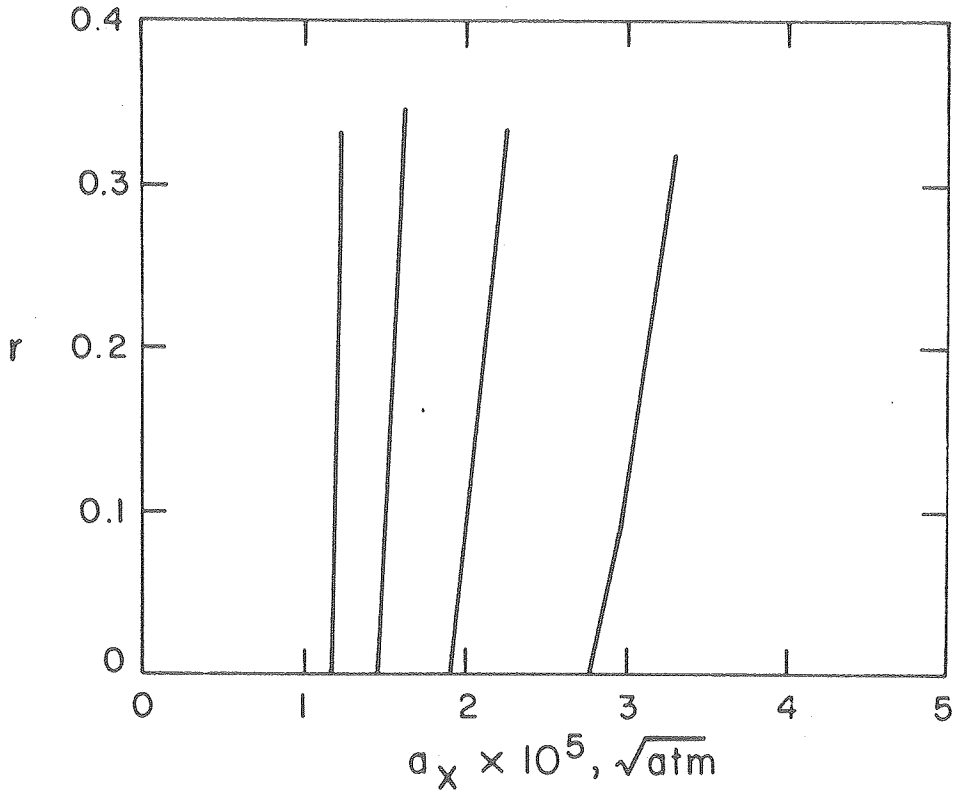

N_B°	0.2	0.4	0.6	0.8
$\frac{\partial r}{\partial a_x}$	6.07×10^4	1.00×10^5	2.14×10^5	6.19×10^5
Correlation coefficient	.995	.999	.999	.999

Figure 5

XBL 7911-13264

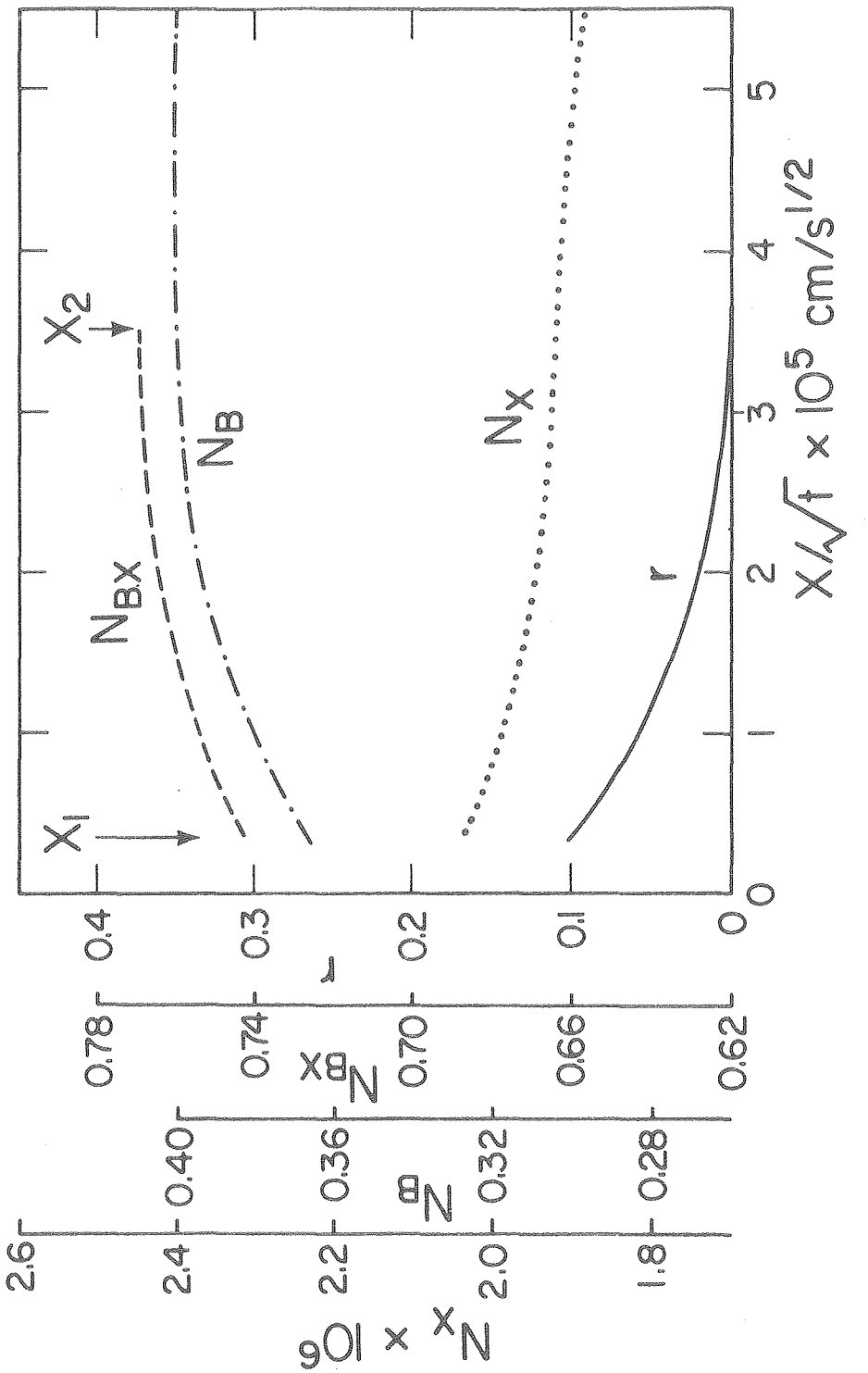

XBL 7912-5100

Figure 6a

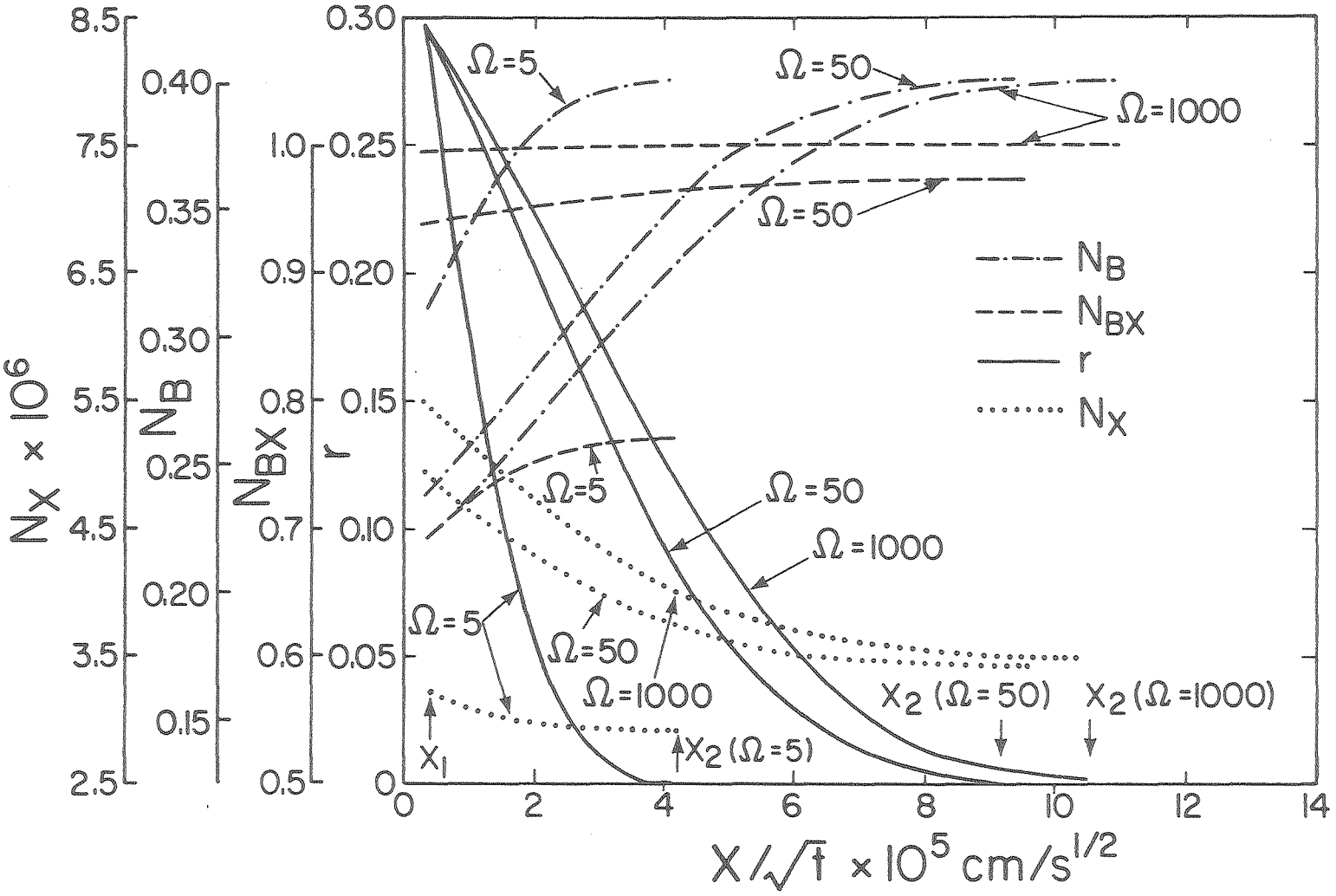

Figure 6b

XBL 7912-5105

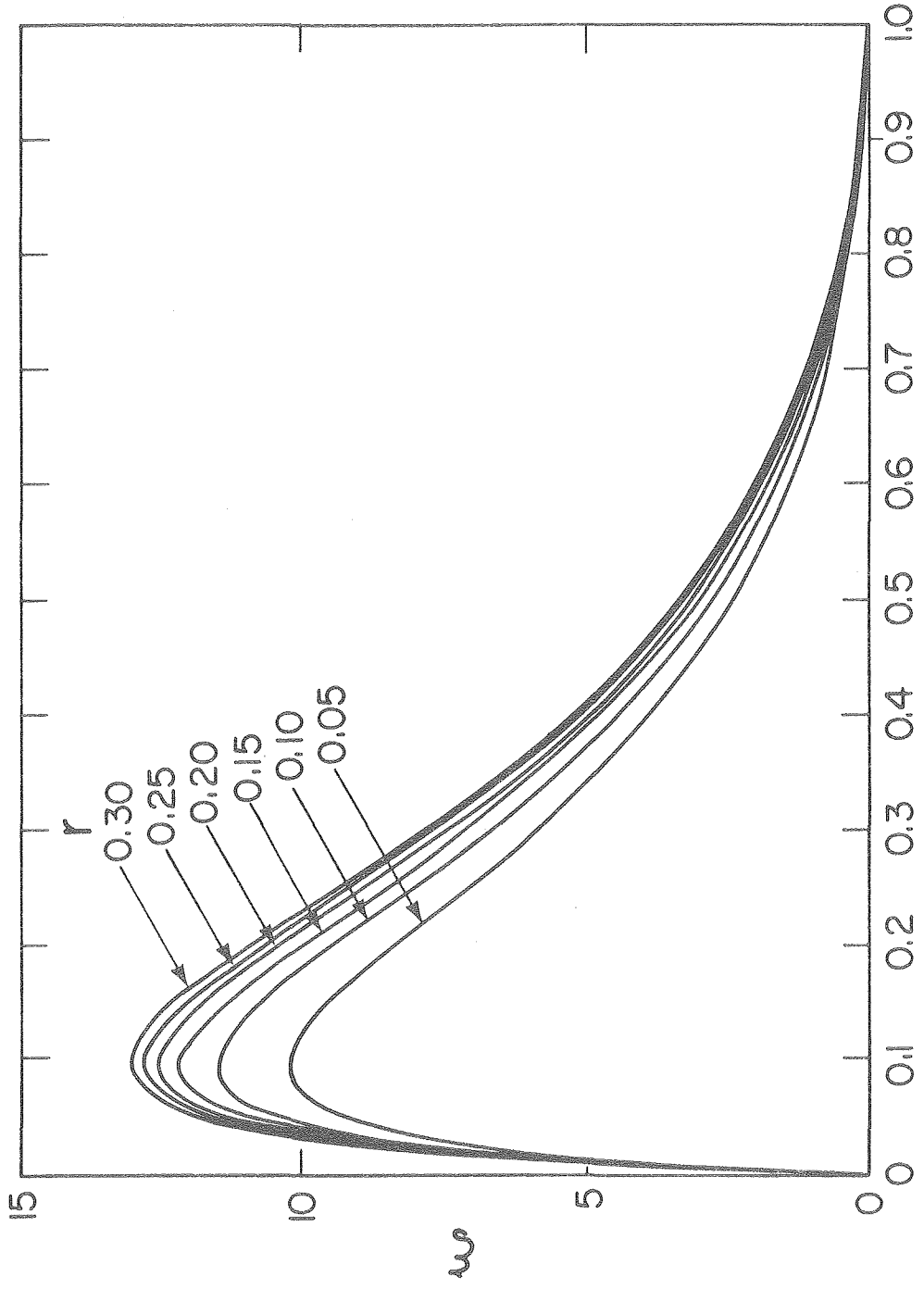

XBL 7912-5102

Figure 7

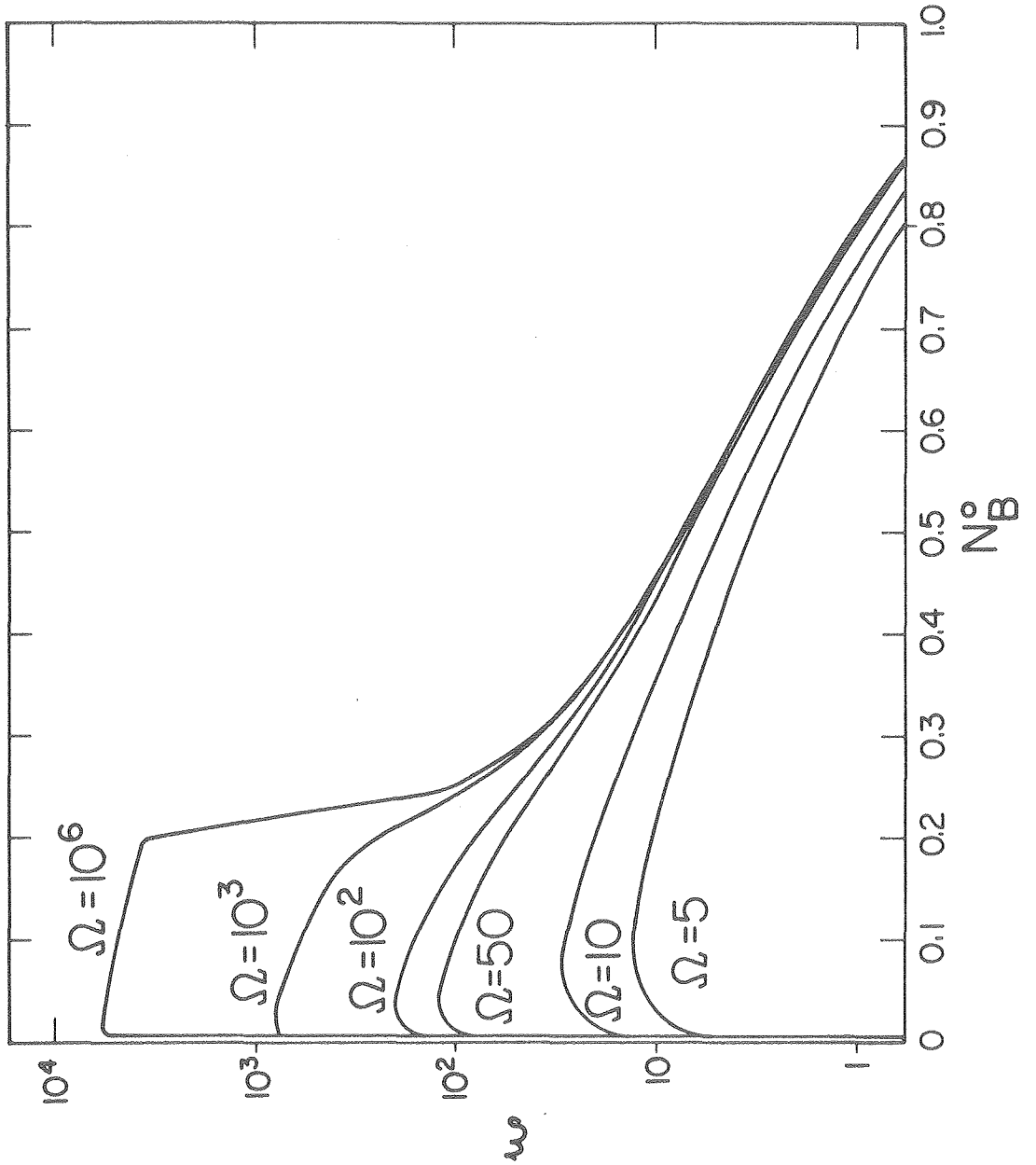

XBL 7912-5103

Figure 8a

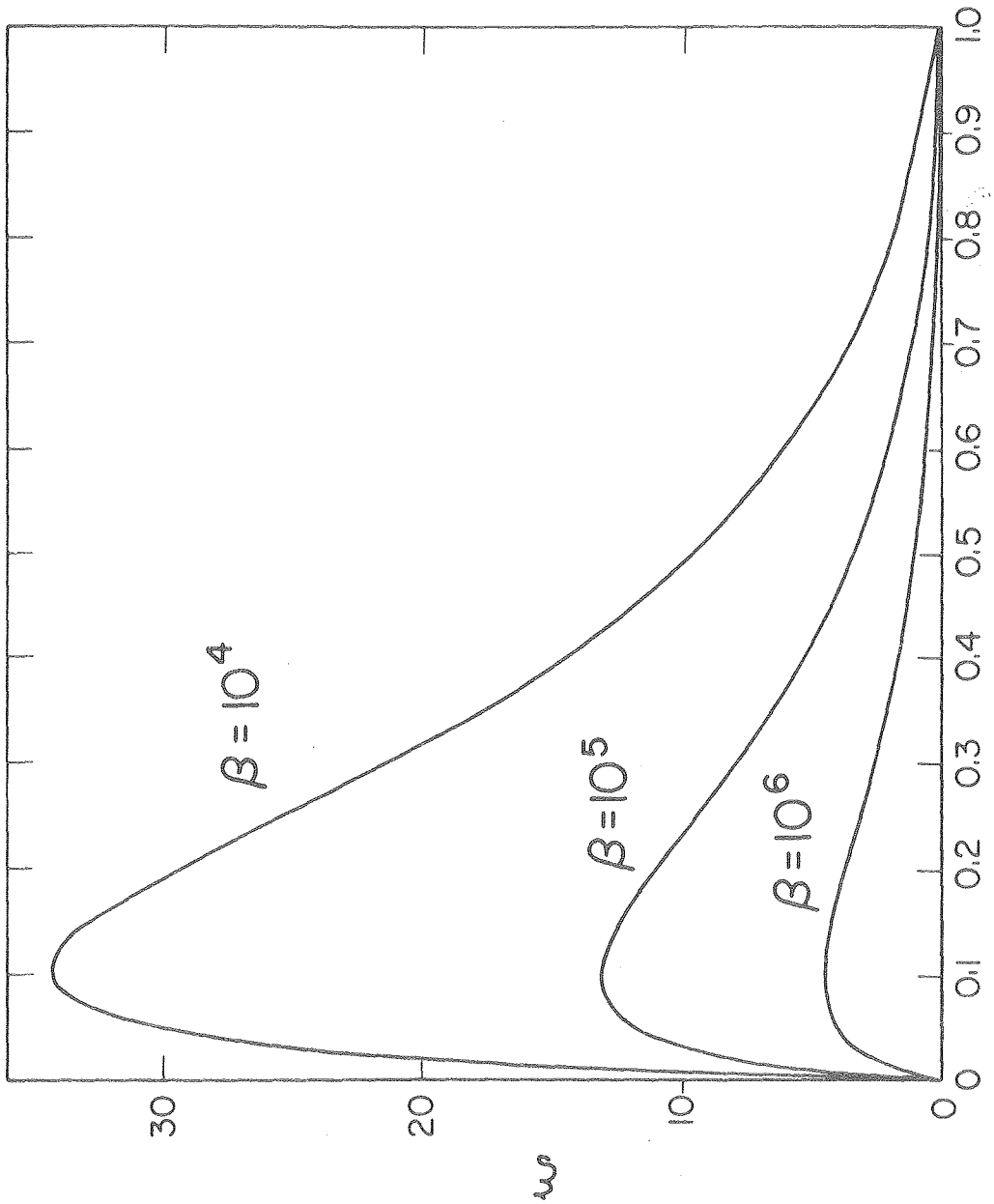

XBL 7912-5104

Figure 8b

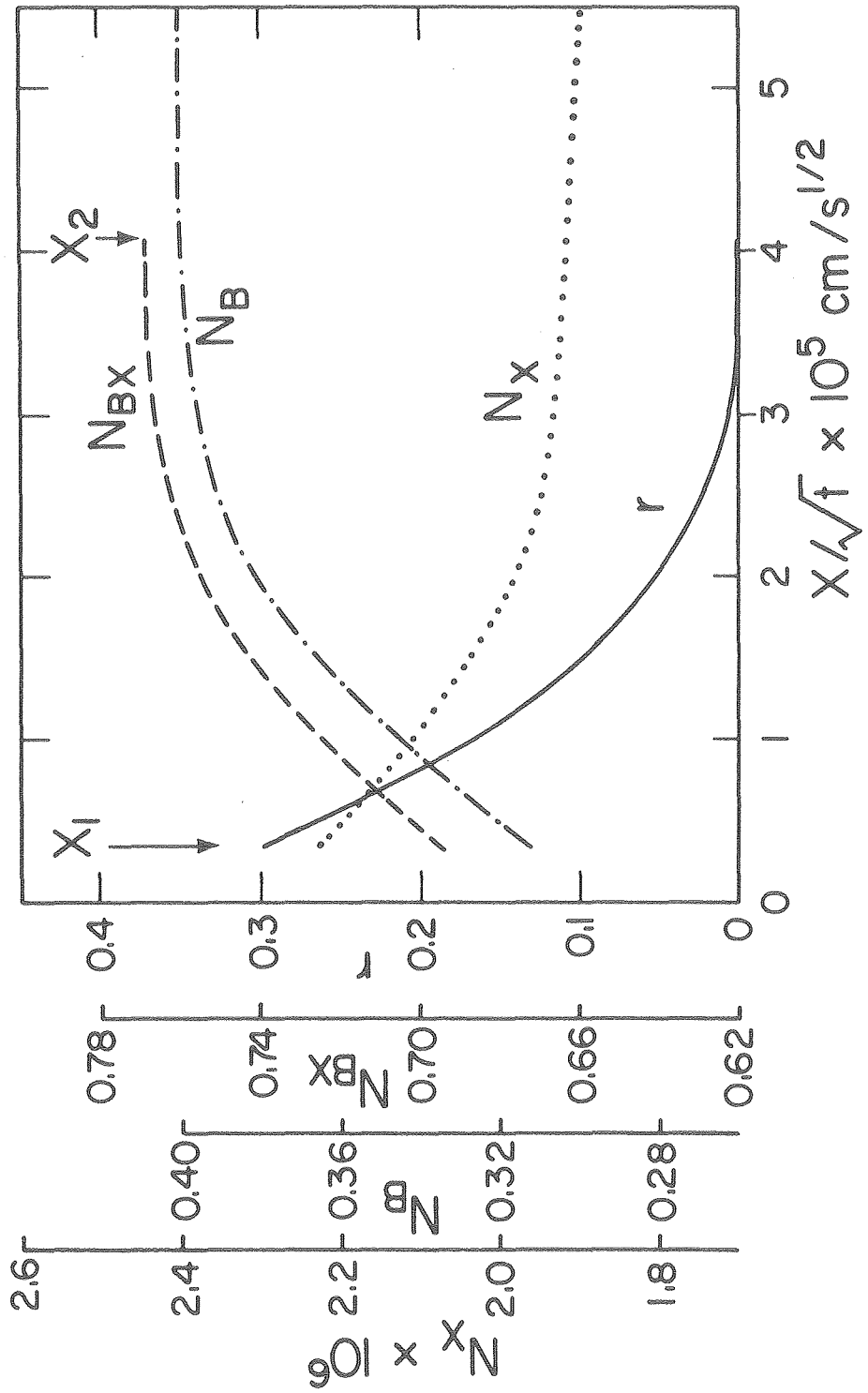
X_1
X_2
N_{BX}
N_B
N_X
r
$X/\sqrt{t} \times 10^5$ cm/s$^{1/2}$
$N_X \times 10^6$
N_B
N_{BX}
r
XBL 7912-5101

Figure 9

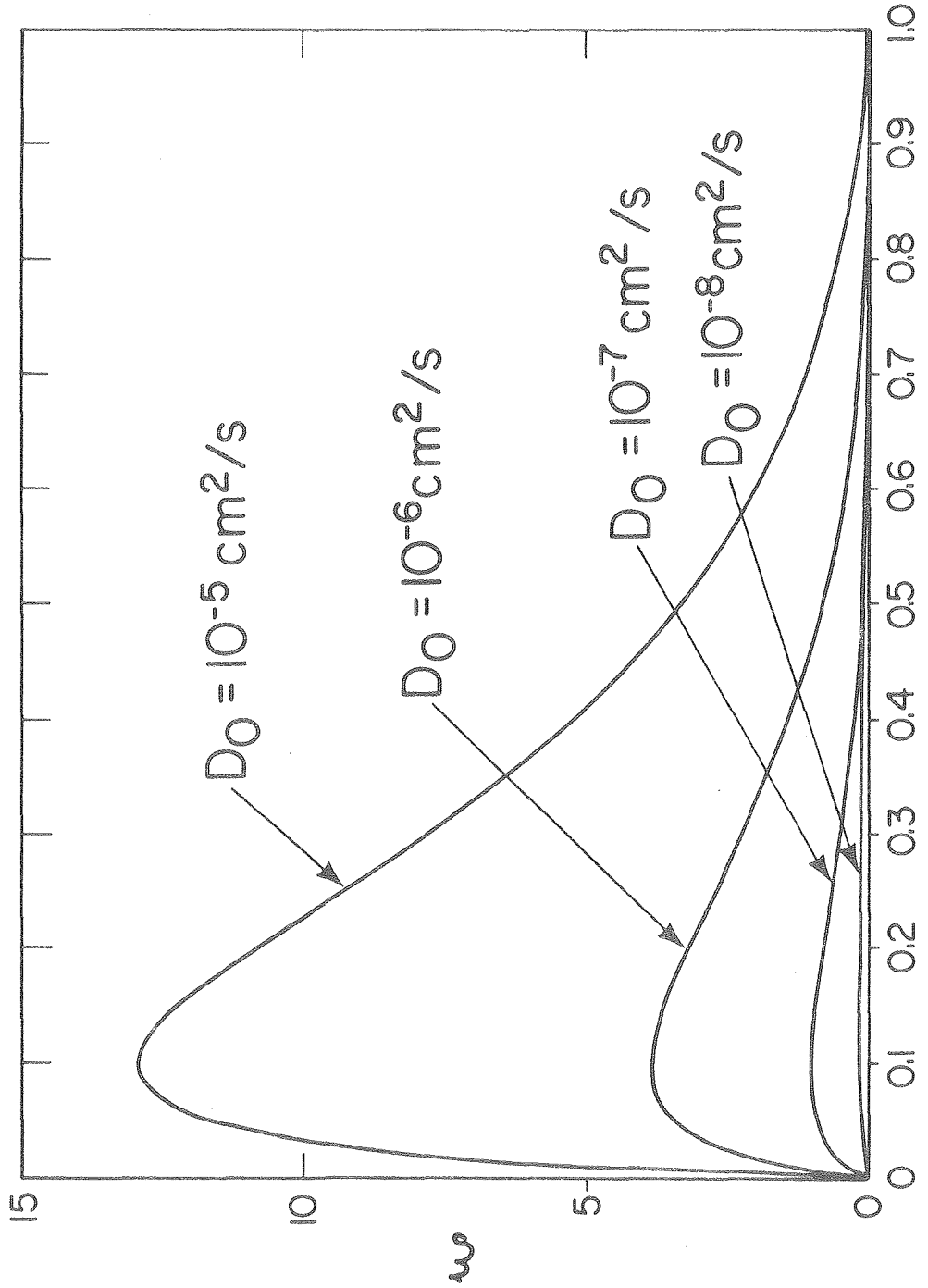

XBL 7912-5106

Figure 10

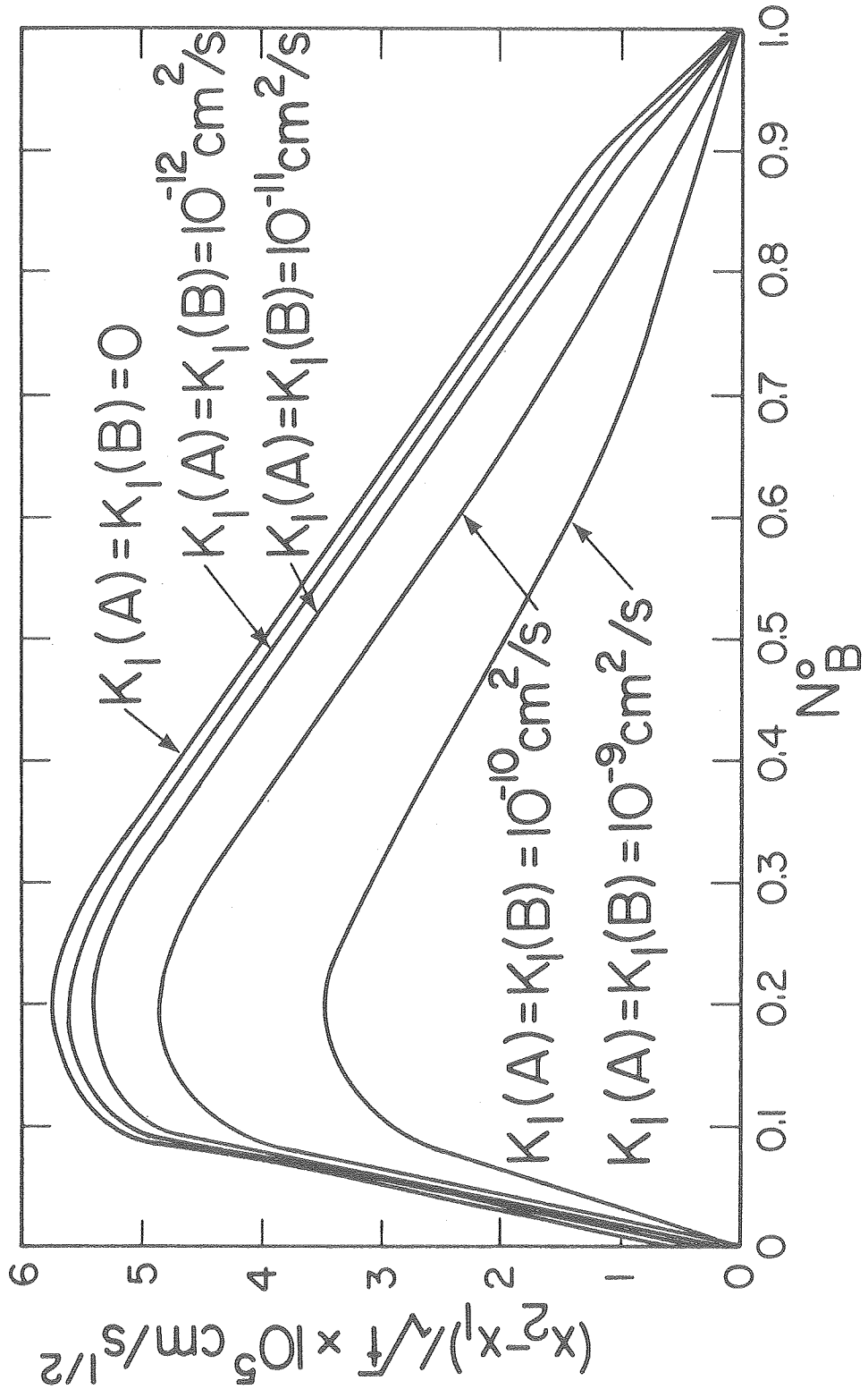

XBL 7912-5107

Figure 11

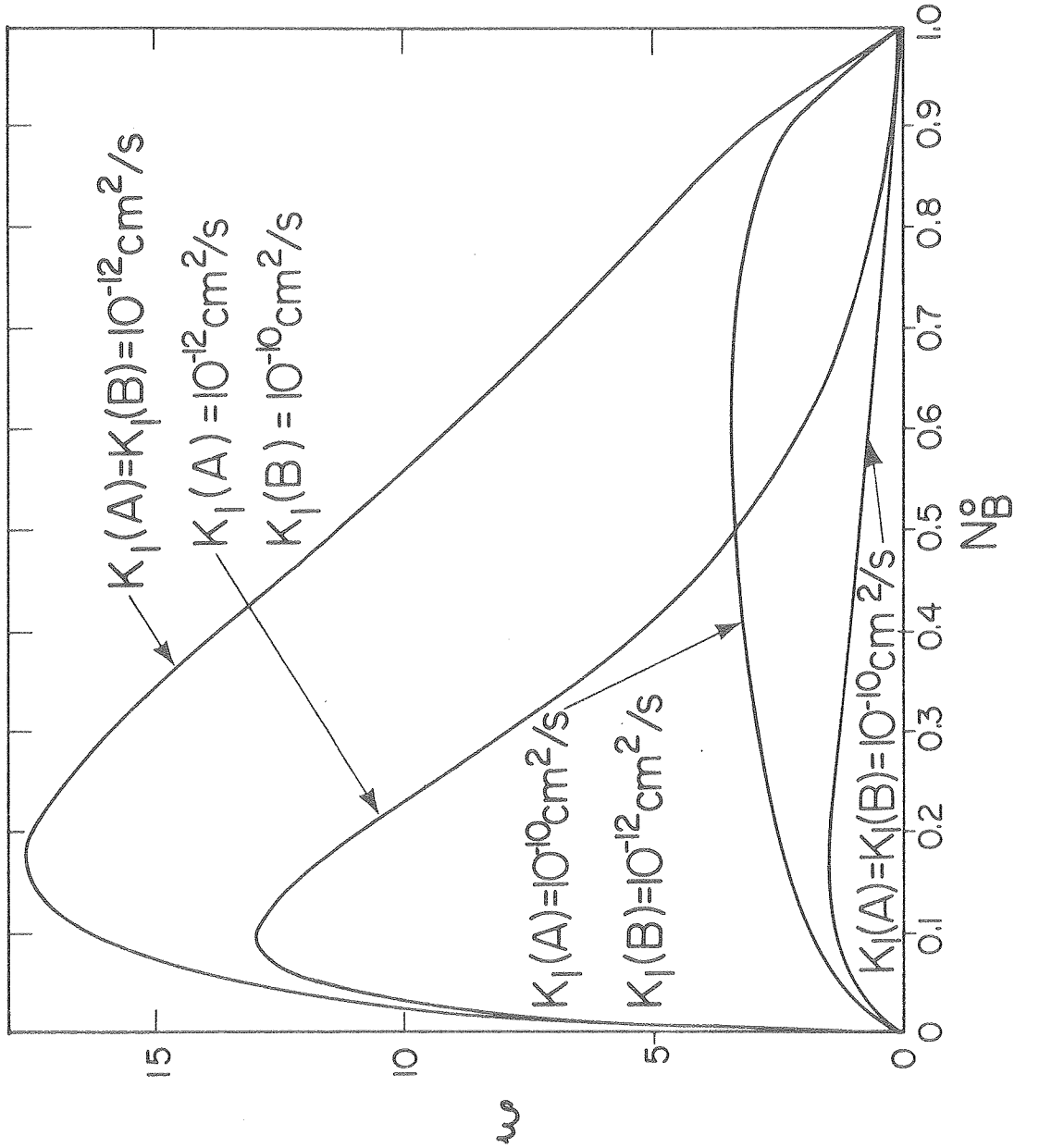

XBL 7912-5108

Figure 12